AIAA SciTech Forum
9 - 13 January 2017, Grapevine, Texas
55th AIAA Aerospace Sciences Meeting

Stall Cell Formation over a Boeing Vertol VR-7 Airfoil

Ata Esfahani*, Nathan Webb† and Mo Samimy‡
Gas Dynamics and Turbulence Laboratory, Aerospace Research Center
The Ohio State University, Columbus, Ohio 43235

The results of experiments to investigate flow control using nanosecond DBD (NS-DBD) plasma actuators over a thin airfoil with an aspect ratio of 3 and leading edge separation at a post-stall angle of attack are presented. The Reynolds number based on the chord was fixed at $5.0 \cdot 10^5$ and the angle of attack was set to 19°. A single actuator was mounted near the leading edge of the airfoil. Fluorescent surface oil flow visualization (FSOFV) and stereo Particle Image Velocimetry (PIV) were employed to investigate any spanwise non-uniformities on the airfoil surface as well as in the flow. The baseline showed some spanwise non-uniformity both on and off the surface. Excitation at low Strouhal numbers ($0.3 < St_e < 0.78$) led to the emergence of spiral nodes near the trailing edge of the airfoil surface and a three-dimensional surface topology (similar to an asymmetric stall cell pattern). Off-surface stereo PIV data suggests, however, that the flow field remains nearly two-dimensional. Excitation at a Strouhal number of 2.04 produces distinct 3D features in the stereo PIV data. Further increases in excitation Strouhal number result in slight acceleration of the flow near the leading edge and formation of two symmetric stall cells. Increasing the excitation Strouhal number even further results in more well-defined stall cells. This effect saturates around $St_e = 6.0$ and further increases in excitation frequency have minimal effects on the stall cells. This is surprising as the scientific community had hitherto believed stall cells to form only over thick airfoils. The results clearly indicate that the instabilities responsible for stall cell formation are present on thin airfoils as well as thick ones and perhaps the lack the appropriate disturbance environment is the reason stall cells have hitherto not been observed on thin airfoils.

I. Introduction

Flow separation imposes considerable performance penalties on lifting surfaces that operate in post-stall regimes. Limitations in flight envelope and loss of control are among the chief reasons for the interest in the research community for better understanding of this phenomenon. This problem is relevant to a wide range of applications from wind turbine to rotorcraft blades and from the wings of super maneuverable fighter aircraft to agile micro air vehicles. The stall characteristics of various airfoil are directly related to their geometry. Thick airfoils are known to undergo a so-called "gentle" stall in the form of trailing edge separation which progressively moves towards the leading edge with increase in the angle of attack. Thin airfoils, on the other hand, display what is commonly referred to as abrupt stall characteristics where a sudden flow separation from leading edge leads to immediate loss of lift[1]. The leading edge radius of curvature dictates the momentum required to maintain attached flow and this shapes the stall behavior of thin and thick airfoils[2]. Emergence of three-dimensional flow features in the post-stall regime further complicates the stall phenomenon and leads to manifestation of effects such as lift and drag variation along the airfoil span[3,4]. As a result, any study in which the flow is assumed to be spanwise-uniform, where three-dimensional features might exist, may lead to under- or overestimation of the loads experienced by the airfoil.

The mushroom-shaped three-dimensional flow features referred to as stall cells have been the subject of investigation for at least 40 years with early reports of their appearance by Gregory et al.[5] dating back to 1971. Further investigation of stall cells by other researchers[6–10] using flow visualization techniques such as tufts and surface oil flow visualization shed light on the conditions in which stall cells emerge and also resulted in derivation of empirical relations that could be used for predicting the number and wavelength of stall cells. A better understanding of the stall

* Graduate Student, AIAA student member
† Research Engineer, AIAA member
‡ The John B. Nordholt Professor of Mechanical and Aerospace Engineering, Director of Aerospace Research Center, AIAA Fellow, Corresponding Author <samimy.1@osu.edu>

cells has been obtained recently through the use of advanced optical diagnostics techniques such stereo PIV and pressure sensitive paints (PSP). Authors such as Manolesos[11], DeMauro et al.[12], Dell'Orso et al.[13], Disotell and Gregory[14], Disotell[15] and Ragni and Ferreira[4] have used planar or stereo PIV, not only to determine the extent of the stall cells, but also to study their temporal evolution, extract frequency content in the reversed flow region, and obtain vorticity distributions and Reynolds stress concentrations. Disotell et al.[16] also used fast-responding PSP to obtain the pressure distribution over a pitching wind turbine blade with stall cells. While advances in flow diagnostics have helped to further understanding of stall cells and their characteristics, the underlying mechanisms that lead to their emergence in post-stall flows are not well-understood.

Early work of Weihs and Katz[7] postulated that the stall cells are formed due to the development of Crow instability[17]. Yon and Katz [18] in their study concluded that shear layer roll up (i.e. the Crow instability) is not the mechanism responsible for the formation of stall cells. Numerical and theoretical work of Rodriguez and Theofilis was aimed at exploring the formation mechanism of stall cells with a different approach[19]. The authors perturbed a low-Reynolds flow with a laminar separation bubble with two- and three-dimensional disturbances. They found that disturbances of any amplitude would induce three-dimensional features as the investigated flow was unstable due to the presence of the shear flow over the reversed flow region. This, in turn, lead to the breakdown of the flow in the spanwise direction and formation of stall cells. More recently, De Mauro et al.[12] and Dell'Orso et al[13]. demonstrated the used of zig-zag tapes as 3D disturbances for inducing stall cells in flow conditions in which stall cells did not appear naturally. Dell'Orso et al. reported that the use of a zig-zag tape covering 30% of the span resulted in the emergence of the stall cells whereas a full-span zig-zag tape did not induce any 3D features[13]. They observed the same effect by a partial span step. When using piezoelectric-driven steps, their phase-locked PIV data indicated the presence of a fully-extended step nearly eliminated the stall cells which formed over the clean airfoil. The unsteady behavior of the flow field in the actuation period where flow alternates between a quasi-two-dimensional and a three-dimensional state and suggests that alternate shedding and shear layer flapping, as reported by Driver et al.[20] might be playing a role. Manolesos and Voutsinals also explored the use of zig-zag tapes in their research but for a different purpose[11]. They found that the use of a limited-span tape can eliminate the jostling motion of the stall cells, as previously reported by Yon and Katz[18]. This was desirable to improve the quality of their stereo PIV experiments. Nevertheless, Dell'Orso et al., based on their experimental results, firmly believe that 3D perturbations are necessary for the creation of stall cells[13]. This opens up the possibility of using various flow control techniques for inducing and potentially controlling stall cells.

Plasma-based actuators due to their wide bandwidth, high amplitude[21–23] and absence of moving parts are promising candidates for implementation of active flow control on airfoils. Dielectric barrier discharge (DBD) actuators are one of the latest additions to the family of plasma actuators[21] that have been the subject of numerous investigations in recent years. DBD actuators driven by AC waveforms impart momentum to the flow, and have demonstrated control authority at relatively low Reynolds numbers. However, scaling their effect for successful implementation in high speed flows requires the use of thicker dielectrics and higher voltages[24–27]. Even when these changes are implemented there is a limit to the effectiveness of DBD actuators driven by AC waveform in high Reynolds number flows.[26]

An alternative, first investigated by Roupassov et al.[28–30] is to drive a single dielectric barrier discharge actuator with high voltage nanosecond DC pulses at various frequencies. These actuators (NS-DBD) have demonstrated control authority at relatively high flow speeds[30–37] as their control mechanism is not momentum-based. Several studies conducted by Roupassov et al.[28,30], Che at al.[38], Popov at al.[39], Correale et al.[40], Starikovskii et al.[41] Little et al.[37] and Takashima et al.[42,43] demonstrated that nanosecond pulse driven DBD actuators primarily affect the flow through generating rapid, localized Joule heating that can excite the instabilities in the flow. This leads to the generation of coherent structures which promote mixing and alter the flow structure.[44–47]. A distinctive signature of the rapid localized heating generated by the mentioned actuators is the generation of compression waves that originate near the discharge[41,42,44,46]. These waves have been reported to be formed by discharge filaments[41,46,48] but it is not clear whether they significantly contribute to the control authority of the NS-DBD actuators[44]. Reports by Correale at al.[40] and Dawson et al.[46] indicate that the strength of the compression waves strongly depends on discharge voltage.

Our previous study concentrated on exploring the merits of low- and high-frequency, $St_e \approx$ O(1) and O(10) respectively, excitation of high-Reynolds number separated flows on a thin rotorcraft typical airfoil using NS-DBD actuators[49]. An important aspect of the previous study that differentiates it from the works done on NS-DBD actuators hitherto is the implementation of these actuators on a thin, asymmetric airfoil with leading edge separation. Reports of the studies conducted by Little et al.[33,50], Correale et al.[40] and Rethmel et al.[35] on thick airfoils (NASA EET and NACA 0015, respectively) point to the effectiveness of excitation at lower Strouhal numbers $St_e \approx$ O(1). In addition, in the small existing body of work on NS-DBD actuators, the merits of excitation at higher Strouhal numbers, mentioned in the works of Amitay and Glezer[51] and Glezer et al.[52], have not been previously explored and therefore

there was no information on how the flow would respond when forced by an NS-DBD actuator at high frequencies. While our data confirmed the existence of a significant difference in the flow response for low- and high-frequency excitation, as previously reported by Glezer et al. and Amitay et al.[51–55], we also noticed a growing disparity between surface pressure and PIV data (collected at different spanwise planes) as the excitation frequency increased. Due to optical access limitations, the streamwise PIV results were not acquired at a mid-span location where the pressure taps are located. It has been assumed the flow would be two-dimensional and uniform in the spanwise direction. This assumption was reinforced by the results of the works of Bragg et al.[9] and Disotell and Gregory[15] where the authors suggested that stall cells would emerge only on thick airfoils which display trailing edge separation. The disparity between surface pressure and PIV data on our thin airfoil suggested otherwise. A limited series of fluorescent surface oil flow visualization experiments in conjunction with pressure sensitive paint (PSP) measurements confirmed the existence of stall cells over the airfoil for various excitation frequencies.

This work seeks to explore the three-dimensional flow features that emerge on a thin, post-stall airfoil as a result of instability excitation by NS-DBD actuation, and potential control opportunities. Development of 3D features is studied using fluorescent surface oil flow visualization and stereo PIV. The data is also compared with streamwise planar PIV data. The implications of the findings and the role of excitation of instabilities that lead to the emergence of stall cells are then discussed.

II. Experimental Facility and Techniques

A. Airfoil and Facility

Experiments were performed in the recirculating wind tunnel located at the Gas Dynamics and Turbulence Laboratory, within the Aerospace Research Center at The Ohio State University. The tunnel has an optically clear acrylic test section measuring 610×610 mm in cross-section and 1220 mm in length. A Boeing Vertol VR-7 airfoil was used as it is a typical airfoil used in rotorcraft. The composite airfoil has a chord of c =20.3 cm and is mounted in the center of the test section between two acrylic disks, giving it an aspect ratio AR = 3. The disks are able to rotate continuously, allowing for any angle of attack. The tunnel is capable of producing a continuous range of flow velocities from 3 – 95 m/s. Further details may be found in the works of Esfahani et al.[49] and Clifford et al.[56]. The angle of attack investigated here was 19° at a chord-based Reynolds number of $5.0 \cdot 10^5$ which corresponds to a freestream velocity of approximately 37 m/s. The freestream turbulence intensity is on the order of 0.25% of the freestream velocity at this Reynolds number.

A single coordinate system, shown in Figure 1, is used throughout this paper. The origin is at the airfoil leading edge. The system is a two-dimensional grid aligned with the test section where streamwise, normal, and spanwise axes are normalized by the chord, denoted x/c, y/c, and z/b, respectively.

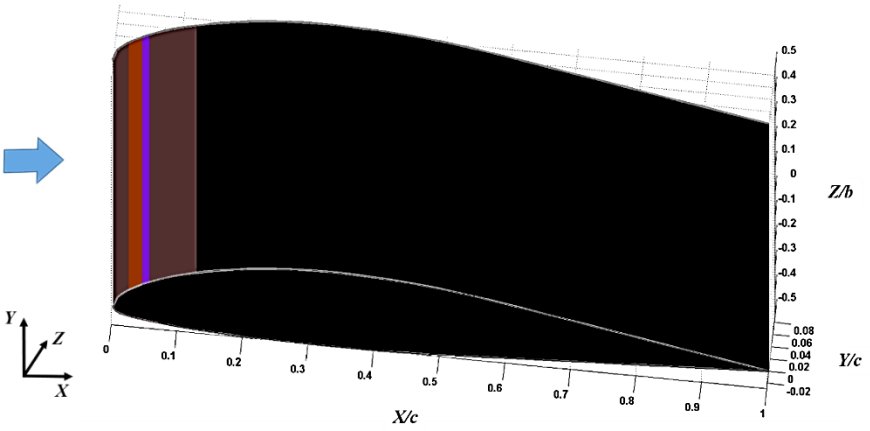

Figure 1. Schematic of the airfoil, coordinate system, and actuator location.

B. DBD Actuator and Pulser

A single actuator was placed close to airfoil leading edge. The actuator is constructed of two 0.09 mm thick copper tape electrodes; the exposed high-voltage electrode is 6.35 mm (0.25 in) wide and the covered ground electrode is 12.70 mm (0.50 in) wide. The dielectric layer is composed of three layers of Kapton tape, each 0.09 mm thick with a

dielectric strength of 10 kV. The total thickness of the entire actuator is 0.45 mm. The actuator was placed on the suction side of the airfoil with the electrode junction at $x/c = 0.04$. This location was just upstream of the separation location as determined by surface oil flow visualization. The actuator is powered by an in-house custom-built pulse generator. The pulse generator utilizes a magnetic compression circuit to create the input waveform for the actuator. A DC power supply supplying 450 VDC is used to power the pulse generator. The specifics of the pulse generator are discussed in previous work by Clifford et al.[56] and Takashima et al.[42,43].

Representative discharge characteristics were acquired for a ~570-millimeter-long actuator driven at f_e =100 Hz corresponding to St_e = 0.54 ($St_e = f_e c/U_\infty$). The instantaneous voltage and current traces of a typical representative discharge in addition to the power and energy traces are plotted in Figure 2. The peak voltage was 10 kV and the peak current was 36 A. The peak power consumption was 335 kW. However due to the narrow pulse width, the steady state energy consumption was 12.6 mJ per pulse. For the frequencies considered (less than St_e = 15), this corresponds to a time averaged power of 10 W. At the testing conditions, this corresponds to 3% of the freestream energy.

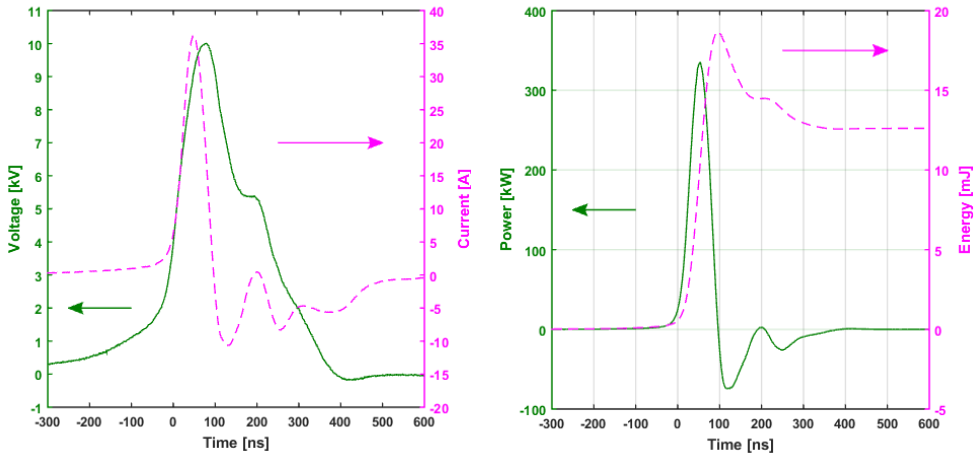

Figure 2. Traces of instantaneous (a) current and voltage (b) power and energy.

C. PIV Setup

PIV was the primary diagnostic technique. PIV data were acquired for both the flow passing over the suction side of the airfoil and downstream of the trailing edge. Seed particles were injected upstream of the test section. Extra virgin olive oil was atomized using a TSI 6-jet atomizer (model 9306A). The light source is a Spectra Physics PIV-400 double-pulsed Nd:YAG laser. The laser beam is formed into a sheet with the use of a 1 m focal length spherical lens and one 25 mm focal length cylindrical lens. Various turning optics were used to direct the laser sheet into the wind tunnel. The laser sheet has a thickness of ~2mm and is located at z/b = 0. 05 for the planar PIV measurements.

To acquire streamwise data over the airfoil and in the wake region, a two-camera setup (shown in Figure 3) comprised of two LaVision 12-bit 2048×2048 px Imager Pro cameras, each with a Nikon Nikkor 35 mm f/1.2 lens was employed. The cameras were positioned 253 mm center to center on a horizontal optical rail. The lenses of the cameras were located ~980 mm away from the laser sheet. The cameras acquired data simultaneously at an average acquisition rate of 3.3 Hz. For excited cases, five sets of 100 image pairs were taken for a given case (due to actuator runtime limitations), whereas for the baseline data, a single set of 1000 images were taken. A limited series of experiments aimed at characterizing coherent structures over the airfoil were carried out using a single-camera setup that employed a La Vision Imager Pro X 4M camera with a 50 mm lens. Two sets of 250 image pairs per data point were acquired at a rate of 5 Hz with this camera.

A stereo cross stream PIV setup, seen in Figure 4, was employed to investigate flow non-uniformities in the spanwise direction. The stereo PIV setup was comprised of two 5.5 Mpx, 16 bit LaVision Imager sCMOS cameras. Each camera was fitted with a 24 mm, wide-angle Nikon Nikkor f/2.8 lens in order to maximize the field of view. Approximately 89% of the airfoil span was imaged with this setup. The angle between the camera sensor normal vector and the tunnel centerline was approximately 37°. One set of 600 image pairs was acquired at a rate of 10.5 Hz for each data point.

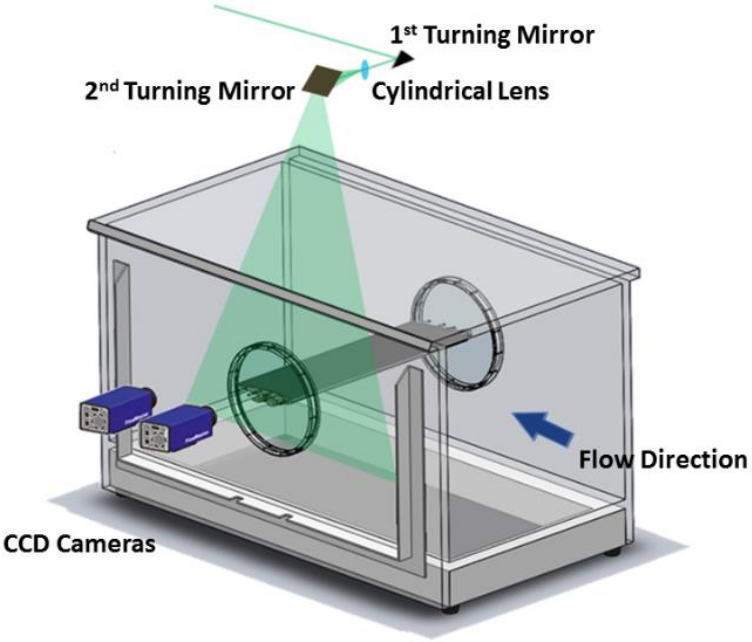

Figure 3. Schematic of the dual-camera streamwise planar PIV setup.

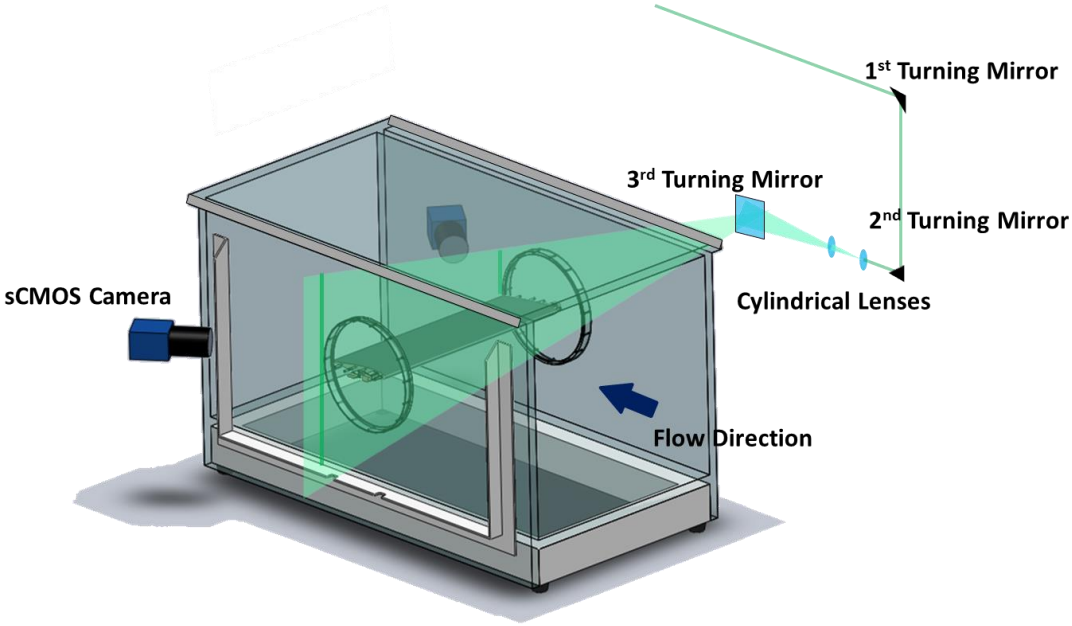

Figure 4. Schematic of spanwise stereo PIV setup showing the laser sheet location downstream of the airfoil trailing edge.

D. Fluorescent Surface Oil Flow Visualization

Fluorescent surface oil flow visualization (FSOFV) was employed in order to study the flow topology over the airfoil under various conditions. A mixture of 10,000 and 350 cSt silicone oil (3 parts 10,000 cSt oil and 7 parts 350 cSt oil) with a viscosity of approximately 1000 cSt was used to hold the fluorescent pigments. The viscosity of the oil

was chosen to allow the observation of the separation line unsteadiness traces and simultaneously prevent excessive amounts of the mixture from flying off of the model.

The UV pigments had an average diameter of 5 to 20 μm and could be excited by visible light. Two 1000 W LED flood lights were used to illuminate the mixture (as shown in Figure 5) in 10 s intervals. The procedure for acquiring the images was as follows: first the angle of attack was set and the tunnel was brought up to speed. As soon as the desired conditions were established in the tunnel, the actuators were turned on. The final pattern was usually established after 6 minutes of run time. Laboratory lights would then be turned off and a DSLR camera would be used to acquire the images in low-light conditions.

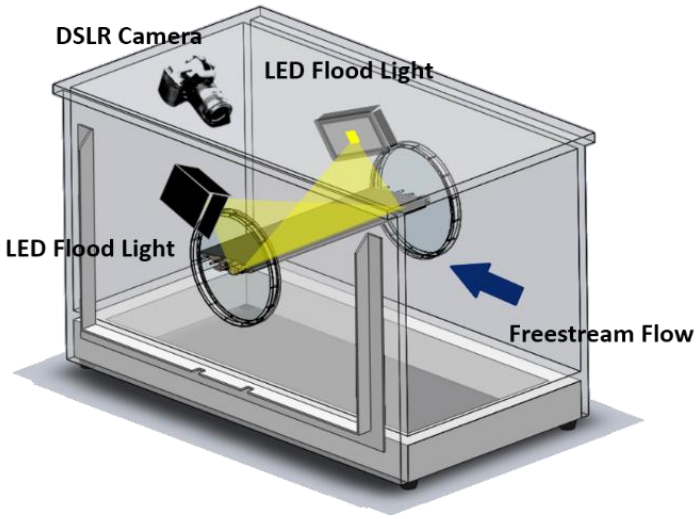

Figure 5. Schematic of the surface oil flow visualization setup.

E. Static Pressure

Static pressure measurements on the airfoil surface were acquired using three Scanivalve digital pressure sensor arrays (DSA-3217). A total of 35 taps are located on the surface of the airfoil and the tap distribution is shown in Figure 6. As indicated by the figure, 3 taps are covered by the plasma actuator. The pressure coefficient, $C_p = (p - p_\infty) / q_\infty$, was averaged over 300 samples acquired at 1 Hz near the centerline. The sectional lift coefficient was calculated using the line integral $C_L = -\int_{-1}^{1} C_p \sin\theta \, ds$, where θ is the surface-normal angle and ds is the arc length.

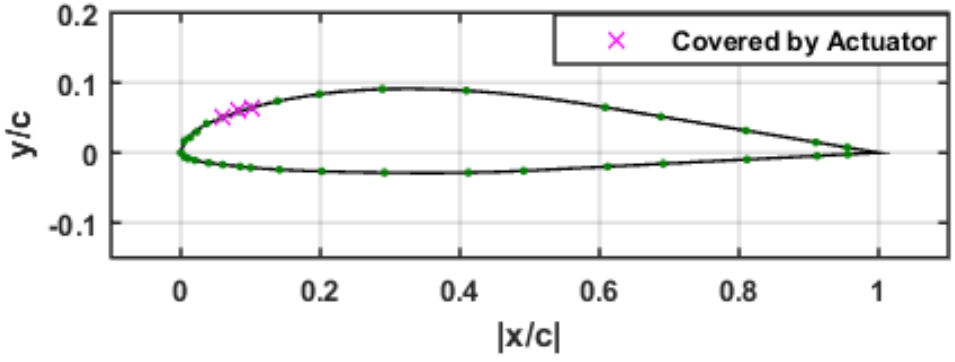

Figure 6. Static pressure tap distribution over the airfoil.

III. Results and Discussion

The lift coefficient as a function of angle of attack for several Reynolds numbers for the baseline model (with actuators installed but off) is shown in Figure 7. It is evident that the stall angle for the VR-7 airfoil at a Reynolds number of $5.0 \cdot 10^5$ (and $1.0 \cdot 10^6$) is 16°. As expected, the airfoil demonstrates typical stalling behavior of thin airfoils[1,2] in the form of a rapid drop in lift coefficient C_l due to abrupt leading edge flow separation. While this occurs at all tested Reynolds numbers, the effects are less severe at $Re = 1.0 \cdot 10^6$. Manolesos and Voutsinas[11] combined stereo PIV and CFD simulation results to offer a model of the vortex system over an airfoil when a stall cell is present. They proposed three types of vortices in such a flow field: a bent and deformed shear layer spanwise vortex, a trailing edge spanwise vortex, and a pair of streamwise vortices that impinge on the airfoil surface and create the so-called spiral nodes commonly observed in SOFV experiments. Spalart[3] in his analysis of "lift cells" used lifting line theory to suggest that the destabilizing interaction between the wing and trailing vortices leads to the appearance of stall cells when $\frac{dc_l}{d\alpha} < 0$. This suggestion agrees with early observations of Yon and Katz[18] on a thick NACA 0015 airfoil where a two-cell pattern was formed at shallow post-stall angles. Disotell and Gregory[57] and Disotell[15] also stated that stall cells are typically formed at shallow post-stall angles on thick airfoils, as confirmed by earlier studies of Broeren and Bragg[9].

All of the experiments in this report have been conducted at an angle of attack of $\alpha = 19°$ where, as shown in Figure 7, $\frac{dc_l}{d\alpha} > 0$. Compared to the findings of Yon and Katz[18] for a NACA 0015, this is well outside the "stable" angle of attack region expected for the emergence of stall cells. Additionally, according to Spalart's analysis[3], wing-vortex interactions are self-correcting for spanwise variations in this region; therefore, the appearance of stall cells in not likely.

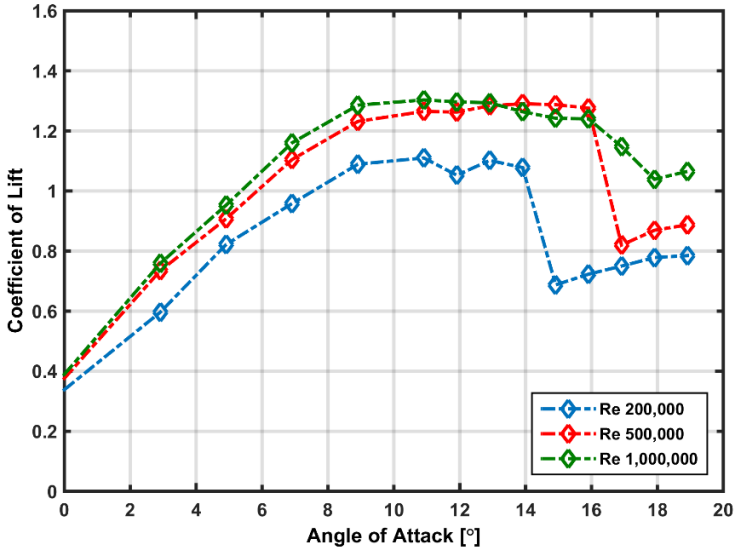

Figure 7. Variation of lift coefficient (C_L) versus angle of attack for different Reynolds numbers.

The PIV and FSOFV results for the airfoil at several excitation conditions are presented in Figure 8 and Figure 9, respectively. These results show the separation line and surface flow topology on the airfoil and the velocity field just downstream of the airfoil trailing edge (see Figure 4). The baseline separation line is clearly three-dimensional, and the flow field appears to be weakly three-dimensional as well. Such separation fronts have been observed previously[12,13,57] and are believed to be precursors to the development of well-defined stall cells. Weak spiral nodes at $z/b = 0$ and -0.4 may be present in the FSOFV image of the baseline (Figure 9). When the flow is excited at $St_e = 0.6$ strong spiral nodes appear on the surface of the airfoil at positions consistent with the baseline. Their presence would typically indicate that stall-cell associated streamwise vortices embedded in the shear layer are present over the airfoil. Furthermore, the spanwise location of the spiral nodes suggest that these potential stall cells are asymmetric. However, the PIV results depict a very two-dimensional flow. In fact, it appears to be more two-dimensional that the baseline case, in which only a hint of spiral nodes is present. At first glance these results may seem contradictory, however, the actuators introduce dynamics which do not typically accompany stall cells. The natural shedding over the airfoil

occurs at a Strouhal number of St = 0.6 and our previous work has shown that excitation introduced at that frequency results in the shedding of strong and very coherent spanwise vortices[49]. A plausible explanation is that these vortices are preventing the three-dimensionality from moving away from the wall, up into the flow. This hypothesis, if correct, would explain the reason for the apparent discrepancy between the PIV and FSOFV results.

When the flow is excited at St_e = 10.73 the FSOFV results indicate that the separation line moves further downstream and the shape of the separation line becomes more symmetric. Unlike in the St_e = 0.6 case, the surface topology is in agreement with the flow data from the PIV measurement. Both clearly show a symmetric, three-dimensional separation with two stall cells. This result supports the working hypothesis (that coherent shedding due to excitation causes the apparent discrepancy in the St_e = 0.6 results), as our previous work[49] has shown that high-frequency excitation produces small structures which quickly disintegrate and dissipate upstream of the trailing edge. What is more striking about the St_e = 10.73 case is the observed asymmetry. Several models of stall cell spanwise arrangement and wavelength have previously been proposed[7,8,15,58]. However, while the observed three-dimensionality in the baseline and St_e = 0.6 cases agree with some of these models, none appropriately predicts the arrangement observed in the St_e = 10.73 case. Clearly this flow has atypical characteristics; in addition to the apparent presence of stall cells in a flow where previously thought improbable. Significant further research must be conducted to begin to understand these differences and their sources.

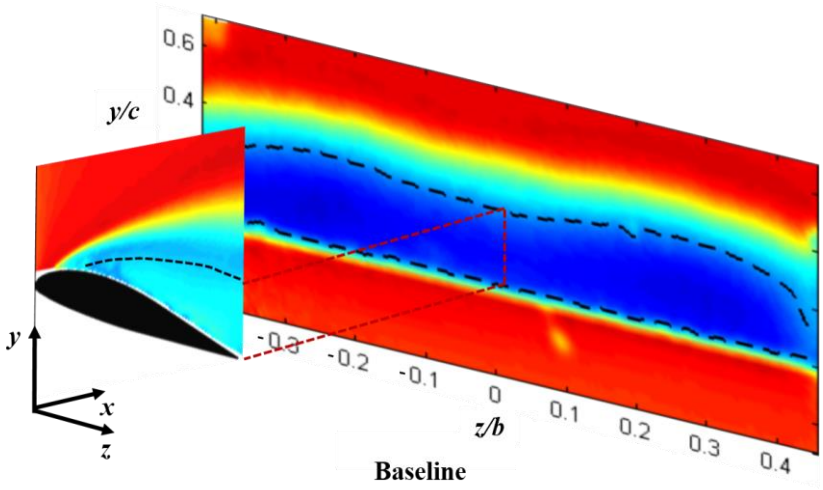

(a)

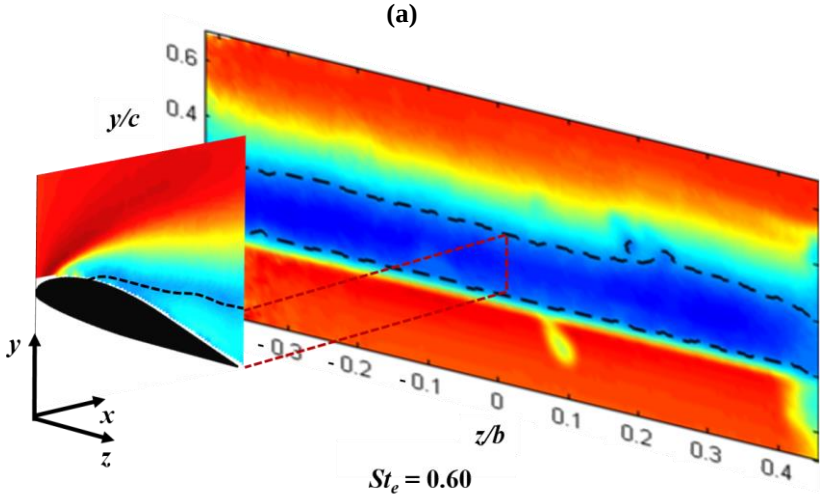

(b)

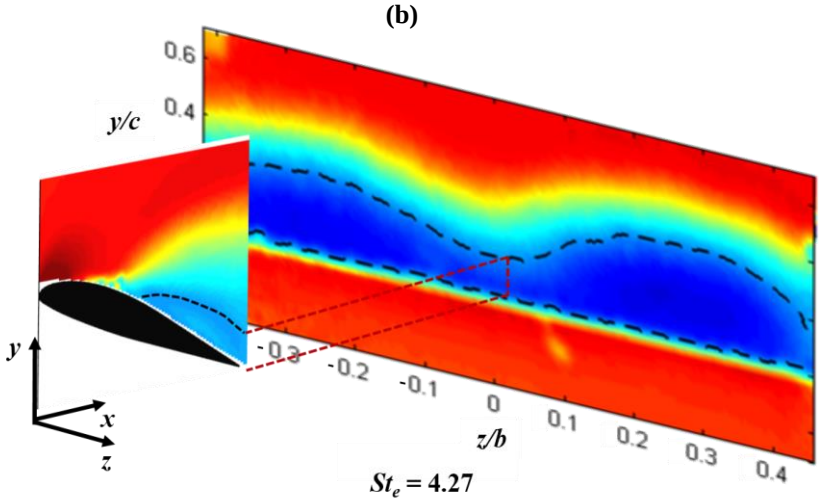

(c)

Figure 8. Comparison of normalized streamwise velocity on a cross-stream plane at x/c =1.05 and on a streamwise plane at z/b = 0.05 for (a) baseline, (b) low-frequency excitation, and (c) high-frequency excitation. Dashed black lines indicate the zero streamwise velocity contour.

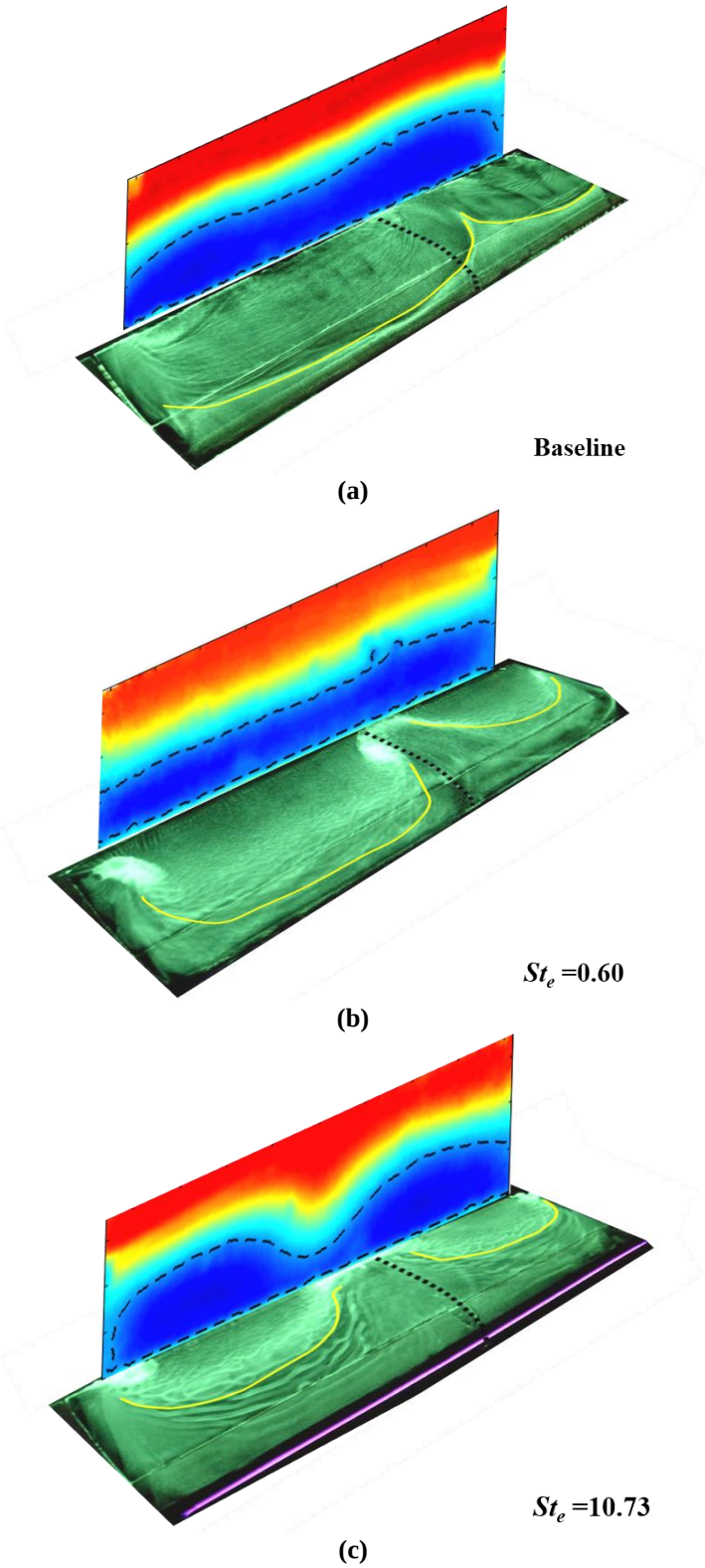

Figure 9. Comparison of normalized streamwise velocity on a cross-stream plane at x/c =1.05 and fluorescent surface oil flow visualization for (a) baseline, (b) low-frequency excitation, and (c) high-frequency excitation. Dashed black lines indicate the zero streamwise velocity contour. Dotted black lines on the surface depict the location of pressure taps.

Another important aspect of the global flow field in the presence of stall cells is the pressure distribution over the airfoil. In particular, the validity of the 2D assumption by virtue of which the pressure data is acquired only at mid-span of the airfoil for calculating the lift generated by the entire airfoil must be assessed. The location of the surface pressure taps used to acquire the data shown in Figure 10 is indicated by black dotted lines in the FSOFV images of Figure 9. While the pressure taps are well within the separated flow region in the baseline case, they are situated between the stall cells when the flow is excited at either St_e = 0.6 or St_e = 4.27.

Manolesos and Voutsinas argue that since the streamwise vortices associated with stall cells merely bend and distort the trailing edge vortex line[4,11], the flow can still be separated outside the stall cells. A careful examination of the spanwise PIV data of Figure 8 indicates that flow is still separated at z/b = 0. Pressure data from Figure 10 also suggests that this is the case (though the fact that several pressure taps are covered by the actuators prevents emphatic statements). The nearly flat distribution of C_p for the excitation Strouhal numbers below around 4.27 suggests that despite some acceleration of the near-wall flow at several excitation frequencies due to enhanced mixing, the flow is still separated, downstream of the first uncovered pressure tap (at x/c = ???). In contrast, the sharp suction peaks observed around leading edge for high-frequency excited cases suggests that the flow is attached at the leading edge (at least at the airfoil centerline). The FSOFV and streamwise planar PIV measurements shown in Figure 8 and Figure 9 also support these conclusions. The VR-7 airfoil is a thin airfoil which generates the majority of its lift near the leading edge. Thus, the presence of stall cells close to the leading edge likely introduces spanwise variations in lift, while a further downstream location of the separation line suggests that the airfoil will not experience major variations in the spanwise loading. As such, errors resulting from the calculation of aerodynamic loads for the entire airfoil based on mid-span measurements will likely be greater in cases where the separation (and associated three-dimensionality) is near the leading edge.

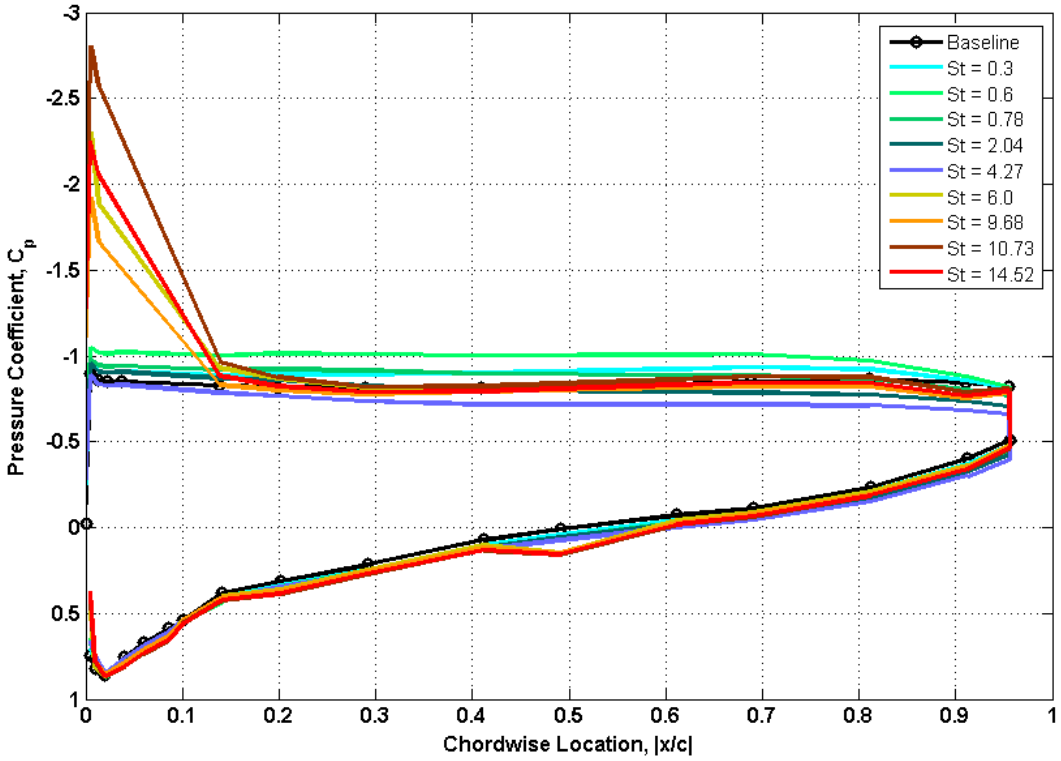

Figure 10. C_p distribution for the baseline and excited cases.

After examining the general flow structure, the details of the effect of excitation frequency on the flow field were investigated. Ensemble-averaged maps of normalized streamwise and vertical velocity downstream of the trailing edge at x/c =1.05 for baseline and excited cases are presented in Figure 11 and Figure 12 respectively. The vertical velocity maps in Figure 12 are overlaid with vectors of the total in-plane velocity to provide an indication of the spanwise

velocity component. Dashed black lines indicate zero streamwise velocity and can be used to assess the separation height at each spanwise location.

As previously observed, the baseline distribution of streamwise velocity is primarily two-dimensional, but possesses a slight three-dimensionality which, when considered in conjunction with FSOFV data in Figure 9 may be a precursor to the formation of stall cells. Exciting the flow at St_e = 0.3 and 0.6 results in a nearly two-dimensional distribution of velocity as seen in Figure 11b and c. This uniformity, as previously hypothesized, is suggested to be caused by the coherent spanwise structures shed when excitation is introduced around the natural shedding frequency of the stalled airfoil. As expected in the presence of strong spanwise structure (and the enhanced mixing), the magnitude of the reverse velocity is decreased by this excitation. This hypothesis is further supported by the elevated level of vertical velocity in the shear layer, which is indicative of the presence of the strong spanwise structures and shedding which are known to be present under these excitation conditions.

As the excitation Strouhal number increases, the flow takes on a well-defined three-dimensional organization. Additionally, the magnitude of the peak reversed flow in each of the stall cells increases as the excitation induced structures become smaller and less coherent, and the associated mixing enhancement decreases. The decrease in the vertical velocity (as seen in Figure 12) with increasing excitation frequency is also in agreement. It is worth noting that, in some cases, the right-hand stall cell height is greater than that of the left-hand stall cell. This asymmetry has been previously noted by the stall cell community, but its origin, as yet, not well understood.[6,12–14,59] While the height of the stall cells increases with increasing excitation frequency, the separation height between them actually decreases. This matches what has been observed by the streamwise planar PIV data (Figure 8) and further illustrates the need to explore how and where stall cells arise, so that appropriate measurement techniques can be employed.

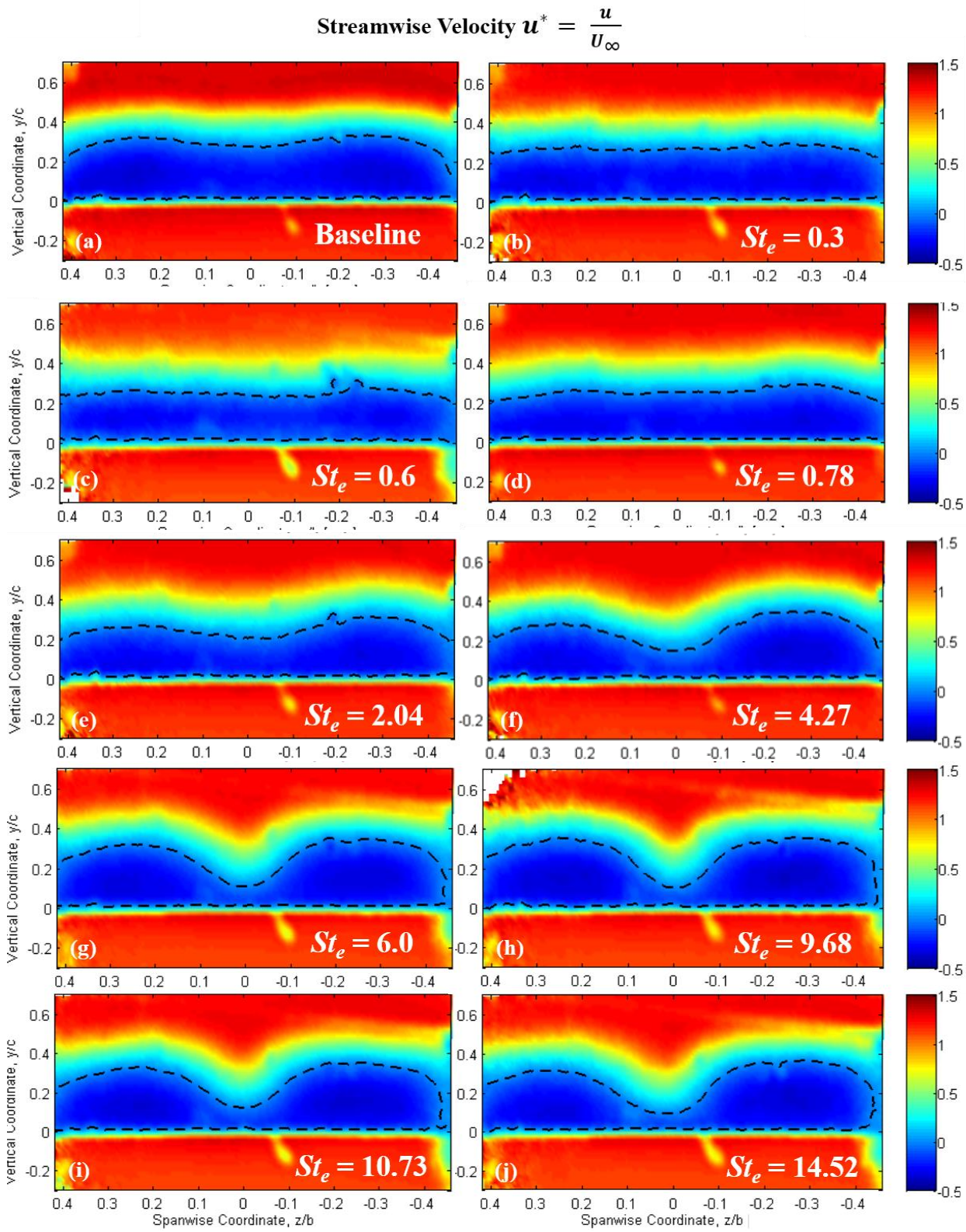

Figure 11. Normalized streamwise velocity on a cross-stream plane at x/c =1.05 for various excitation Strouhal numbers. Dashed black lines indicate the zero streamwise velocity contour.

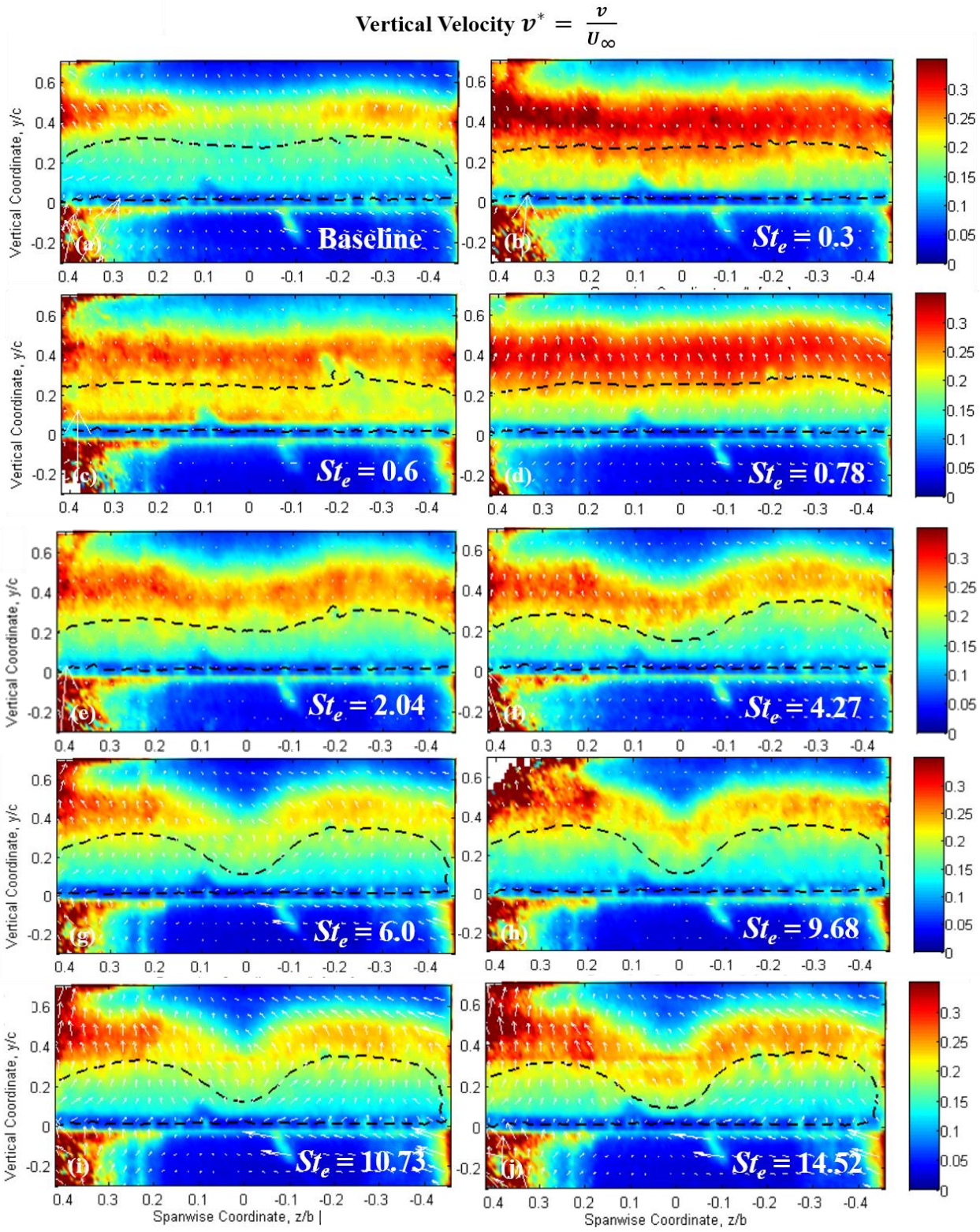

Figure 12. Normalized vertical velocity on a cross-stream plane at x/c =1.05 for various excitation Strouhal numbers. Dashed black lines indicate the zero streamwise velocity contour.

IV. Conclusions

The results of experiments designed to investigate the three-dimensional flow field emerging over a thin, post-stall airfoil are presented. While existing literature suggests that stall cells may be observed only over thick airfoils in shallow stall, the current data suggests that appropriate disturbance environments are conducive to the emergence of stall cells even over thin airfoils in deep stall. The global features of the three-dimensional flow fields were investigated primarily with streamwise planar and spanwise stereo PIV. Complimentary FSOFV data were also collected to map the surface flow topology over the airfoil. The flow was excited using NS-DBD actuators at a wide range of excitation Strouhal numbers. The three-dimensional separation line and slight three-dimensionality observed in the PIV data suggested that a precursor to stall cells may be present in the baseline. Low-frequency excitation led to the emergence of well-defined spiral nodes on the airfoil surface, but a very two-dimensional flow field immediately downstream of the trailing edge. Based on our current and recent results the cause of this discrepancy may be the influence of very coherent spanwise vortices developed in the shear layer over the separated flow by excitation of instability at near the natural shedding Strouhal number. The presence of these strong spanwise vortices may confine the three-dimensionality to the near-surface region. High-frequency excitation resulted in the emergence of distinct, mushroom-shaped stall cells over the airfoil. The magnitude of the reversed flow in the cells was also increased due to inefficient transport of momentum across the shear layer as a result of early breakdown of the small-scale structures by excitation of instabilities at higher Strouhal numbers. These results suggest that the perturbation environment created by the NS-DBD actuators to excite the instabilities associated with the streamwise vortices of stall cells is responsible for the emergence of stall cells in flow conditions where the appearance of such features was previously believed unlikely. These findings, therefore, open up the possibility of employing NS-DBD actuators as flow diagnostic as well as control devices to allow the study of conditions that are conducive to the emergence of stall cells. Therefore, better understanding of the underlying mechanisms of stall cell appearance, which has proved to be elusive to date, and subsequently, effective control, are possible with the use of appropriate disturbance environments created by excitation.

Acknowledgments

This earlier part of this study was sponsored by the Army Research Laboratory with Dr. Bryan Glaz and by the Army Research Office with Dr. Matthew Munson. Helpful discussion provided by the members of the Gas Dynamics and Turbulence Laboratory and Prof. Igor Adamovich is much appreciated.

References

[1] Mccullough, G. B., and Gault, D. E., "Examples of Three Representative Types of Airfoil-section Stall at Low Speed," Sep. 1951.

[2] Greenblatt, D., and Wygnanski, I., "Effect of Leading-Edge Curvature on Airfoil Separation Control," *Journal of Aircraft*, vol. 40, 2003, pp. 473–481.

[3] Spalart, P. R., "Prediction of Lift Cells for Stalling Wings by Lifting-Line Theory," *AIAA Journal*, vol. 52, 2014, pp. 1817–1821.

[4] Ragni, D., and Ferreira, C., "Effect of 3D stall-cells on the pressure distribution of a laminar NACA64-418 wing," *Experiments in Fluids*, vol. 57, Aug. 2016, p. 127.

[5] Gregory, N., "Progress report on observations of three-dimensional flow patterns obtained during stall development on aerofoils, and on the problem of measuring two-dimensional characteristics," 1971.

[6] Winkelman, A. E., and Barlow, J. B., "Flowfield Model for a Rectangular Planform Wing beyond Stall," *AIAA Journal*, vol. 18, 1980, pp. 1006–1008.

[7] WEIHS, D., and KATZ, J., "Cellular patterns in poststall flow over unswept wings," *AIAA Journal*, vol. 21, 1983, pp. 1757–1759.

[8] Boiko, A. V., Dovgal, A. V., Zanin, Y. B., and Kozlov, V. V., "Three-dimensional structure of separated flows on wings (review)," *Thermophysics and Aeromechanics*, vol. 3, Jan. 1996, pp. 1–13.

[9] Broeren, A. P., and Bragg, M. B., "Spanwise Variation in the Unsteady Stalling Flowfields of Two-Dimensional Airfoil Models," *AIAA Journal*, vol. 39, 2001, pp. 1641–1651.

[10]Schewe, G., "Reynolds-number effects in flow around more-or-less bluff bodies," *Journal of Wind Engineering and Industrial Aerodynamics*, vol. 89, Dec. 2001, pp. 1267–1289.
[11]Manolesos, M., and Voutsinas, S. G., "Study of a stall cell using stereo particle image velocimetry," *Physics of Fluids (1994-present)*, vol. 26, Apr. 2014, p. 045101.
[12]Demauro, E. P., Dell'Orso, H., Sivaneri, V., Tuna, B., and Amitay, M., "Measurements of 3-D Stall Cells on 2-D Airfoil," *45th AIAA Fluid Dynamics Conference*, American Institute of Aeronautics and Astronautics, .
[13]Dell'Orso, H., Chan, W., and Amitay, M., "Induced Stall Cells on a NACA0015 Airfoil using Passive and Active Trips," *8th AIAA Flow Control Conference*, American Institute of Aeronautics and Astronautics, .
[14]Disotell, K. J., and Gregory, J., "Time-Resolved Measurements of Cellular Separation on a Stalling Airfoil," *53rd AIAA Aerospace Sciences Meeting*, American Institute of Aeronautics and Astronautics, .
[15]Disotell, K. J., "Low-Frequency Flow Oscillations on Stalled Wings Exhibiting Cellular Separation Topology," The Ohio State University, 2015.
[16]Disotell, K. J., Nikoueeyan, P., Naughton, J. W., and Gregory, J. W., "Global surface pressure measurements of static and dynamic stall on a wind turbine airfoil at low Reynolds number," *Experiments in Fluids*, vol. 57, May 2016, p. 82.
[17]CROW, S. C., "Stability theory for a pair of trailing vortices," *AIAA Journal*, vol. 8, 1970, pp. 2172–2179.
[18]Yon, S. A., and Katz, J., "Study of the Unsteady Flow Features on a Stalled Wing," *AIAA Journal*, vol. 36, 1998, pp. 305–312.
[19]Rodríguez, D., and Theofilis, V., "On the birth of stall cells on airfoils," *Theoretical and Computational Fluid Dynamics*, vol. 25, Jun. 2011, pp. 105–117.
[20]DRIVER, D. M., SEEGMILLER, H. L., and MARVIN, J. G., "Time-dependent behavior of a reattaching shear layer," *AIAA Journal*, vol. 25, 1987, pp. 914–919.
[21]Moreau, E., "Airflow control by non-thermal plasma actuators," *Journal of Physics D: Applied Physics*, vol. 40, 2007, p. 605.
[22]Samimy, M., Adamovich, I., Webb, B., Kastner, J., Hileman, J., Keshav, S., and Palm, P., "Development and characterization of plasma actuators for high-speed jet control," *Experiments in Fluids*, vol. 37, Aug. 2004, pp. 577–588.
[23]Benard, N., and Moreau, E., "Capabilities of the dielectric barrier discharge plasma actuator for multi-frequency excitations," *Journal of Physics D: Applied Physics*, vol. 43, 2010, p. 145201.
[24]Thomas, F. O., Corke, T. C., Iqbal, M., Kozlov, A., and Schatzman, D., "Optimization of Dielectric Barrier Discharge Plasma Actuators for Active Aerodynamic Flow Control," *AIAA Journal*, vol. 47, 2009, pp. 2169–2178.
[25]Patel, M. P., Ng, T. T., Vasudevan, S., Corke, T. C., Post, M., McLaughlin, T. E., and Suchomel, C. F., "Scaling Effects of an Aerodynamic Plasma Actuator," *Journal of Aircraft*, vol. 45, 2008, pp. 223–236.
[26]Wicks, M., Thomas, F., Schatzman, D., Bowles, P., Corke, T., Patel, M., and Cain, A., "A Parametric Investigation of Plasma Streamwise Vortex Generator Performance," *50th AIAA Aerospace Sciences Meeting including the New Horizons Forum and Aerospace Exposition*, American Institute of Aeronautics and Astronautics, .
[27]Wicks, M., Thomas, F. O., Corke, T. C., Patel, M., and Cain, A. B., "Mechanism of Vorticity Generation in Plasma Streamwise Vortex Generators," *AIAA Journal*, vol. 53, 2015, pp. 3404–3413.
[28]Roupassov, D., Zavialov, I., and Starikovskii, A., "Boundary Layer Separation Plasma Control Using Low-Temperature Non-Equilibrium Plasma of Gas Discharge," *44th AIAA Aerospace Sciences Meeting and Exhibit*, American Institute of Aeronautics and Astronautics, .
[29]Roupassov, D., Starikovskii, A., Nikipelov, A., and Nudnova, M., "Boundary Layer Separation Control by Nanosecond Plasma Actuator," *44th AIAA/ASME/SAE/ASEE Joint Propulsion Conference & Exhibit*, American Institute of Aeronautics and Astronautics, .
[30]Roupassov, D. V., Nikipelov, A. A., Nudnova, M. M., and Starikovskii, A. Y., "Flow Separation Control by Plasma Actuator with Nanosecond Pulsed-Periodic Discharge," *AIAA Journal*, vol. 47, 2009, pp. 168–185.
[31]Marino, A., Catalano, P., Marongiu, C., Peschke, P., Hollenstein, C., and Donelli, R., "Effects of High Voltage Pulsed DBD on the Aerodynamic Performances in Subsonic and Transonic Conditions," *43rd Fluid Dynamics Conference*, American Institute of Aeronautics and Astronautics, .
[32]Peschke, P., Goekce, S., Leyland, P., Ott, P., and Hollenstein, C., "Experimental Investigation of Pulsed Dielectric Barrier Discharge Actuators in Sub- and Transonic Flow," *44th AIAA Plasmadynamics and Lasers Conference*, American Institute of Aeronautics and Astronautics, .
[33]Little, J., Takashima, K., Nishihara, M., Adamovich, I., and Samimy, M., "High Lift Airfoil Leading Edge Separation Control with Nanosecond Pulse DBD Plasma Actuators," *5th Flow Control Conference*, American Institute of Aeronautics and Astronautics, .

[34]Adamovich, I., Little, J., Nishihara, M., Takashima, K., and Samimy, M., "Nanosecond Pulse Surface Discharges for High-Speed Flow Control," *6th AIAA Flow Control Conference*, American Institute of Aeronautics and Astronautics, .
[35]Rethmel, C., Little, J., Takashima, K., Sinha, A., Adamovich, I., and Samimy, M., "Flow Separation Control over an Airfoil with Nanosecond Pulse Driven DBD Plasma Actuators," *49th AIAA Aerospace Sciences Meeting including the New Horizons Forum and Aerospace Exposition*, American Institute of Aeronautics and Astronautics, .
[36]Nishihara, M., Takashima, K., Rich, J. W., and Adamovich, I. V., "Mach 5 bow shock control by a nanosecond pulse surface dielectric barrier discharge," *Physics of Fluids (1994-present)*, vol. 23, Jun. 2011, p. 066101.
[37]Little, J., Takashima, K., Nishihara, M., Adamovich, I., and Samimy, M., "Separation Control with Nanosecond-Pulse-Driven Dielectric Barrier Discharge Plasma Actuators," *AIAA Journal*, vol. 50, 2012, pp. 350–365.
[38]Che, X., Shao, T., Nie, W., and Yan, P., "Numerical simulation on a nanosecond-pulse surface dielectric barrier discharge actuator in near space," *Journal of Physics D: Applied Physics*, vol. 45, Apr. 2012, p. 145201.
[39]Popov, I., Nikipelov, A., Pancheshnyi, S., Correale, G., Hulshoff, S., Veldhuis, L., Zaidi, S., and Starikovskiy, A., "Experimental Study and Numerical Simulation of Flow Separation Control with Pulsed Nanosecond Discharge Actuator," *51st AIAA Aerospace Sciences Meeting including the New Horizons Forum and Aerospace Exposition*, American Institute of Aeronautics and Astronautics, .
[40]Correale, G., Popov, I., Rakitin, A., Starikovskii, A., Hulshoff, S., and Veldhuis, L., "Flow Separation Control on Airfoil With Pulsed Nanosecond Discharge Actuator," *49th AIAA Aerospace Sciences Meeting including the New Horizons Forum and Aerospace Exposition*, American Institute of Aeronautics and Astronautics, .
[41]Starikovskii, A. Y., Nikipelov, A. A., Nudnova, M. M., and Roupassov, D. V., "SDBD plasma actuator with nanosecond pulse-periodic discharge," *Plasma Sources Science and Technology*, vol. 18, 2009, p. 034015.
[42]Takashima, K., Zuzeek, Y., Lempert, W., and Adamovich, I., "Characterization of Surface Dielectric Barrier Discharge Plasma Sustained by Repetitive Nanosecond Pulses," *41st Plasmadynamics and Lasers Conference*, American Institute of Aeronautics and Astronautics, .
[43]Takashima (Udagawa), K., Zuzeek, Y., Lempert, W. R., and Adamovich, I. V., "Characterization of a surface dielectric barrier discharge plasma sustained by repetitive nanosecond pulses," *Plasma Sources Science and Technology*, vol. 20, Oct. 2011, p. 055009.
[44]Leonov, S. B., Petrishchev, V., and Adamovich, I. V., "Dynamics of energy coupling and thermalization in barrier discharges over dielectric and weakly conducting surfaces on μ s to ms time scales," *Journal of Physics D: Applied Physics*, vol. 47, 2014, p. 465201.
[45]Akins, D. J., Singh, A., and Little, J. C., "Effects of Pulse Energy on Shear Layer Control using Surface Plasma Discharges," *45th AIAA Fluid Dynamics Conference*, American Institute of Aeronautics and Astronautics, .
[46]Dawson, R., and Little, J., "Characterization of nanosecond pulse driven dielectric barrier discharge plasma actuators for aerodynamic flow control," *Journal of Applied Physics*, vol. 113, Mar. 2013, p. 103302.
[47]Dawson, R. A., and Little, J., "Effects of pulse polarity on nanosecond pulse driven dielectric barrier discharge plasma actuators," *Journal of Applied Physics*, vol. 115, Jan. 2014, p. 043306.
[48]Peschke, P., Goekce, S., Hollenstein, C., Leyland, P., and Ott, P., "Interaction Between Nanosecond Pulse DBD Actuators and Transonic Flow," *42nd AIAA Plasmadynamics and Lasers Conference*, American Institute of Aeronautics and Astronautics, .
[49]Esfahani, A., Singhal, A., Clifford, C. J., and Samimy, M., "Flow Separation Control over a Boeing Vertol VR-7 using NS-DBD Plasma Actuators," *54th AIAA Aerospace Sciences Meeting*, American Institute of Aeronautics and Astronautics, .
[50]Little, J., and Samimy, M., "High-Lift Airfoil Separation with Dielectric Barrier Discharge Plasma Actuation," *AIAA Journal*, vol. 48, 2010, pp. 2884–2898.
[51]Amitay, M., and Glezer, A., "Role of Actuation Frequency in Controlled Flow Reattachment over a Stalled Airfoil," *AIAA Journal*, vol. 40, 2002, pp. 209–216.
[52]Glezer, A., Amitay, M., and Honohan, A. M., "Aspects of Low- and High-Frequency Actuation for Aerodynamic Flow Control," *AIAA Journal*, vol. 43, 2005, pp. 1501–1511.
[53]Amitay, M., Smith, D. R., Kibens, V., Parekh, D. E., and Glezer, A., "Aerodynamic Flow Control over an Unconventional Airfoil Using Synthetic Jet Actuators," *AIAA Journal*, vol. 39, 2001, pp. 361–370.
[54]Smith, D., Amitay, M., Kibens, V., Parekh, D., and Glezer, A., "Modification of lifting body aerodynamics using synthetic jet actuators," *36th AIAA Aerospace Sciences Meeting and Exhibit*, American Institute of Aeronautics and Astronautics, .

[55] Amitay, M., Horvath, M., Michaux, M., and Glezer, A., "Virtual aerodynamic shape modification at low angles of attack using synthetic jet actuators," *15th AIAA Computational Fluid Dynamics Conference*, American Institute of Aeronautics and Astronautics, .
[56] Clifford, C., Singhal, A., and Samimy, M., "Flow Control over an Airfoil in Fully Reversed Condition Using Plasma Actuators," *AIAA Journal*, vol. 54, 2016, pp. 141–149.
[57] Disotell, K. J., and Gregory, J., "Time-Resolved Measurements of Cellular Separation on a Stalling Airfoil," *53rd AIAA Aerospace Sciences Meeting*, American Institute of Aeronautics and Astronautics, 2015.
[58] Gross, A., Fasel, H. F., and Gaster, M., "Criterion for Spanwise Spacing of Stall Cells," *AIAA Journal*, vol. 53, 2015, pp. 272–274.
[59] Yon, S. A., and Katz, J., "Cellular Structures in the Flow over the Flap of a Two-Element Wing," *Journal of Aircraft*, vol. 35, 1998, pp. 230–232.